Materials Research Proceedings 35 (2023) 135-142 https://doi.org/10.21741/9781644902714-17

Effect of layer and raster orientation on bending properties of 17-4 PH printed via material extrusion additive manufacturing technology

Alessandro Pellegrini[1,a *], Maria Grazia Guerra[1,b], Fulvio Lavecchia[1,c] and Luigi Maria Galantucci[1,d]

[1] Dipartimento di Meccanica Matematica e Management, Politecnico di Bari, Bari, Italy

[a]alessandro.pellegrini@poliba.it, [b]mariagrazia.guerra@poliba.it, [c]fulvio.lavecchia@poliba.it, [d]luigimaria.galantucci@poliba.it

Keywords: Material Extrusion, Stainless steel, Debinding and Sintering, Bending property

Abstract. Material Extrusion (MEX) is one of the most popular Additive Manufacturing technologies. Over the years, the material portfolio has expanded and nowadays, it covers metals such as stainless steels, copper and titanium alloys. The mechanical behaviour of metal parts realized by MEX is of great interest to understand both the potentialities and the limits of the technology. In the present work, a commercial filament of 17-4 PH stainless steel was used as feedstock material to realize four groups of bending specimens obtained by varying the printing direction and the infill line strategy. The main goal of the paper was to evaluate the effect of the above-mentioned factors on the flexural properties. With this purpose, a three-points bending test was performed and results were analysed using the one-way ANOVA approach. The density of the parts was also evaluated.

Introduction

The main Additive Manufacturing (AM) methods to realize metal components are referred to the Laser Powder Bed Fusion (L-PBF) and Directed Energy Deposition (DED). These technologies are energy-intensive, time-consuming, and require high investment costs. Industrial-ready binder-based AM technologies as Material Extrusion Additive Manufacturing (MEX) and Binder Jetting (BJ) have been starting to come an economic alternative to the powder-based technologies [1,2]. The extrusion-based processes allow to avoid raw material loss during the process and to avoid risks for human health due to the release of respirable small particles, because the metal powder is embedded in a filament [3]. Moreover, a lower initial investment for the equipment is required [4]. Metal MEX is a hybrid technology based on the combination of the traditional MEX for polymers and Metal Injection Molding (MIM). From MIM, it inherited the feedstock, which is a mixture of a polymeric binder and metal powder, and the two subsequent phases, named Debinding and Sintering (D&S), for polymer removal and powder sintering, fundamental to obtain a full metal part. After the printing step, the obtained part is defined as green part. This part is a mixture of thermoplastic polymer and metal powder. After the debinding, the part is called brown part and after the last phase, the sintered metal part is obtained [5]. The feedstock, in form of a filament, is composed by a high content of metal powder (from 55 to 90 wt.%) and a polymeric matrix. This latter is constituted by three different components: a main binder (i.e., Polyoxymethylene (POM)), a backbone binder as Polypropylene (PP) and also additives like stearic acid [6]. In literature, the main metallic materials investigated for MEX are stainless steels 316L [4] and 17-4 PH [7] and, more recently, copper [8] and titanium alloys [9] are being investigated.

The entire process chain including the printing, debinding and sintering strongly influences the mechanical performance of parts realized by extrusion-based processes. The difficulty in achieving uniform particle distribution and strong adhesion between the metal powders and polymer matrix [2], the elevated anisotropy due to the printing orientation [10], the high porosity due to presence

Materials Research Proceedings 35 (2023) 135-142 https://doi.org/10.21741/9781644902714-17

of voids occurred during the printing process [11], and the sintering parameters [7] has been highlighted in literature as the main problems of this technology.

Considering the mechanical performance, tensile properties has been extensively investigated [4,10], while the bending properties and the influence of process parameters have been not fully investigated in literature. More in details, Carminati et al. [2] and Thompson et al. [12] tested specimens with previously optimized parameters in order to obtain the best results of flexural stress (σ_f) and deflection. Gonzalez Gutierrez et al. [8] realized bending specimens made of pure copper with different infill percentages and infill patterns. Suwanpreecha and Manonukul [13] and Henry et al. [14] studied the bending proprieties of 17-4 PH parts realized by using the Atomic Diffusion Additive Manufacturing (ADAM) technology. Due to the limitations of a closed software architecture, such as the Markforged one, the comparison was limited to the consideration of different printing orientations. Moreover, in [13] a comparison between as-printed specimens and as-sintered ones was performed.

Referring to the previous works and to the knowledge of the authors, in this work, a commercial 17-4 PH filament was used to manufacture four groups of bending test specimens with a rectangular cross-section, varying the printing direction and the infill line strategy. Two printing directions, flat (XY) and upright (ZX) were selected and two unidirectional infill line strategy (raster direction) were used, 0° and 90°. Three repetitions were realized for each group of specimens. Thus, three-point bending tests were executed on the as-sintered specimens and the data were collected to obtain the average and standard deviation of the investigated flexural properties. The impact of the printing direction and infill line strategies on the flexural properties and density was then evaluated using the one-way ANOVA statistical approach.

Material and Methods

The material used for the manufacture of the specimens was the BASF Ultrafuse® 17-4 PH (BASF 3D Printing Solutions GmbH, Germany). The feedstock is a mixture of a high content of 17-4 PH powder (≃90 wt.%) and a blend of POM+PP. A consumer 3D printer (Henan Creatbot Technology Limited, China) with a ruby nozzle tip of 0.6 mm of diameter was used to manufacture the specimens. The printing parameters, previously optimized, are shown in Table 1 .

Table 1 Printing parameters

Parameters	Value
Infill density (%)	100
Infill line strategy (°)	0 or 90
Wall lines (n°)	2
Printing speed (mm/s)	30
Layer height (mm)	0.15
Flow (%)	120
Nozzle temperature (°C)	260
Bed temperature (°C)	100

To avoid the warpage of the specimens Magigoo® Pro Metal glue stick was adopted. The bending specimens were oversized to compensate the shrinkage that occur after D&S. As reported by the BASF guidelines, the expected shrinkage is 16% for X and Y axes and 20% for Z axis. The dimensions of the sintered parts were reported in Fig. 1a. Fig.1b showed the directions of the infill lines. For a comparison with the literature, two specimens with an alternate infill line of +/-45°, according to the two printing orientation, were printed and sintered

Materials Research Proceedings 35 (2023) 135-142 https://doi.org/10.21741/9781644902714-17

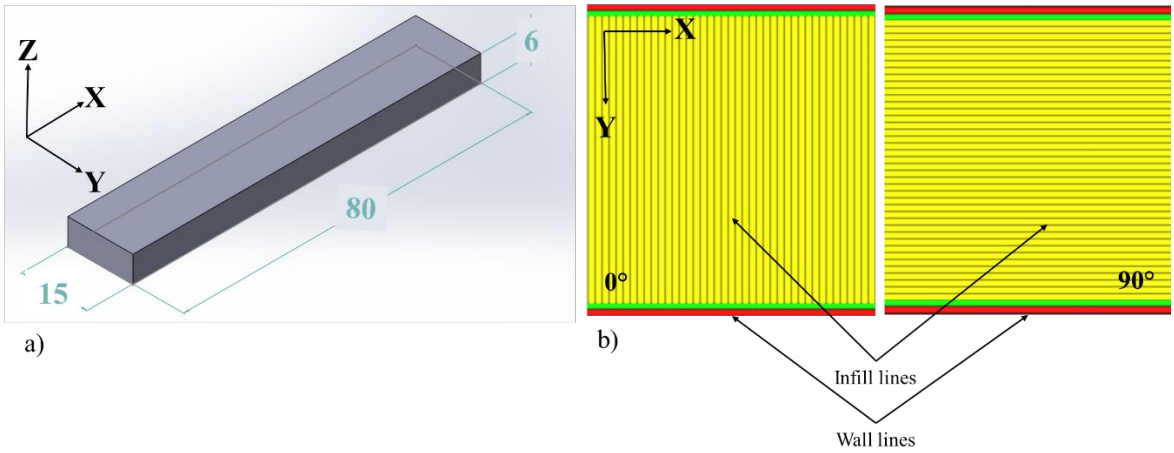

Fig. 1 *a) Dimension of the sintered parts. 2D Scheme of the configuration of the two kinds of infill lines strategy*

Once printed, the specimens' dimensions, such as length (l), width (w) and thickness (t), were measured with using a 3D structured light scanner with a resolution of 0.04 mm and a 100x lens (GOM ATOS Q, Zeiss Corp., Germany). scanner to acquire the main dimensions as length (l), width (w) and thickness (t). The 3D model of the entire specimen (comprising bottom and top faces) was obtained, and it was used for the measurement of volume in the density analysis.

The D&S process was performed according to the manufacturer guidelines (Table 2) and all specimens were debound and sintered on XY plan (Fig. 2).

Table 2 *Debinding and Sintering parameters for BASF Ultrafuse® 17-4 PH*

Phase	Temperature	Holding time	Atmosphere
Debinding	120 °C	Up to 10.5% of weight loss is reached	Nitric acid
Sintering	From room temperature to 600 °C (5°C/min)	1 hours	Hydrogen
	From 600 °C to 1300 °C (5°C/min)	3 hours	

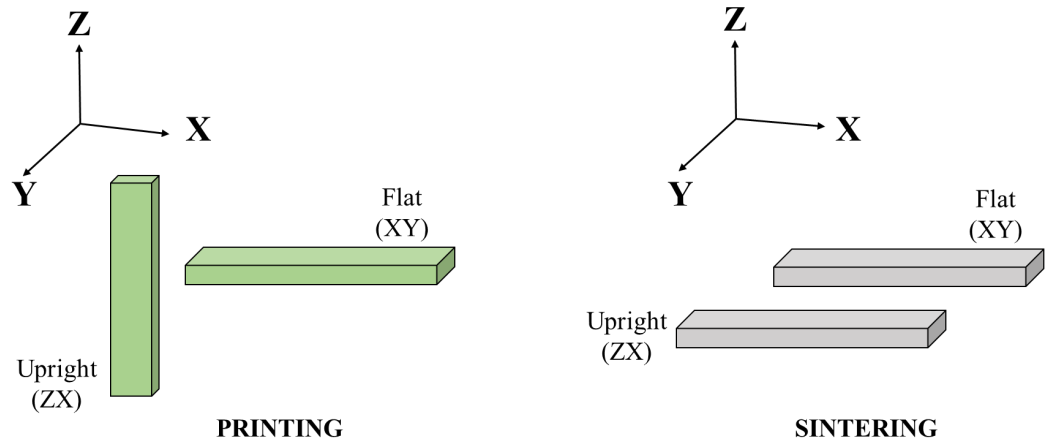

Fig. 2 *Configuration to explain the direction of printing and sintering*

The universal testing machine, Galdabini SUN 10, with a load cell of 100 kN was used for the three-point bending test. A cross head speed of 1 mm/min was selected and a span length of 30 mm was adopted according to the ISO 7438. The contact area between the nose of the punch and the specimens was the last layer (i.e., top layer) for the flat group, instead for the upright specimens was the wide external surface (**Fig. 2**, the plan XY in the "Sintering" configuration).

Materials Research Proceedings 35 (2023) 135-142 https://doi.org/10.21741/9781644902714-17

Results and Discussions

Density evaluation

Starting from the obtained 3D model and using the GOM Inspect software, the volume of each specimen was evaluated, while the mass was measured using a precision balance. The ratio between these two parameters (mass/volume) enable to obtain the density both for the green parts and sintered parts. In Table 3 the green and sintered density were reported. For a comparison, other two specimens called XY-45 and ZX-45 were added for comparison.

Table 3 *Density values for specimens in green and sintered condition*

Group	Green density (g/cm^3)	Sintered density (g/cm^3)
XY-0	4.31±0.02	7.12±0.04
XY-90	4.27±0.02	6.87±0.10
XY-45	4.29	7.08
ZX-0	4.35±0.01	7.13±0.02
ZX-90	4.47±0.01	7.37±0.01
ZX-45	4.40	7.23

From a first analysis, the densities evaluated in each condition did not differ significantly. In the as-printed condition, the average value was between 4.3-4.5 g/cm^3. In the as-sintered condition, instead, except for the XY-90 group, the density was above 7.0 g/cm^3. As a general comment, the upright specimens were denser than flat ones. Using the Pareto chart (Fig. 3a-b), it was possible study deeper this topic. In **Fig. 3**a-b was confirmed the influence of the printing direction both on the green parts and sintered parts, followed by the interactions between printing direction and infill line strategy. Less relevant the effect of the infill line strategy on the sintered density, with respect to the green one, where it was appeared influencing. The difference between the results obtained green and sintered density can be related to the sintering process. After sintering the shrinkage of the parts could form some defects not present in the green condition as delamination between wall lines and infill lines [8], as observed in the following section, or some defect already existent in the green condition as the printing voids induced by the extrusion process [10]. All these defects negatively influence the density and the mechanical performance of the sintered parts.

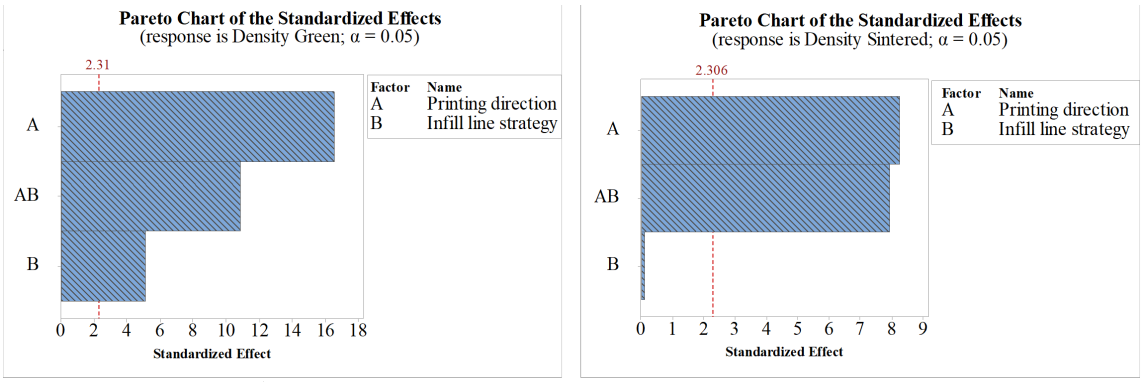

a) b)

Fig. 3 *Pareto chart for a) Green Density b) Sintered Density*

The **Table 4** was reported as summary for the parameters investigated (green density and sintered density) with the different p-value obtained from the ANOVA.

Table 4 *Summary table of the p-value for each parameter investigated.*

Term	p-value Green density	p-value Sintered density
Printing direction	0.000	0.000
Infill line strategy	0.000	0.916
Printing direction*Infill line strategy	0.001	0.000

Materials Research Proceedings 35 (2023) 135-142 https://doi.org/10.21741/9781644902714-17

Bending properties

The data obtained from the bending test were the load (F) and the stroke of crosshead. Using Eq.2 it was possible derive the flexural stress (σ_f). The thickness and width used for the calculation of σ_f were derived from the analyses with GOM Inspect, instead the span length (s_l) was defined by the standard ISO 7438 equal to 30 mm.

$$\sigma_f = \frac{3Fs_l}{2wt^2} \quad (2)$$

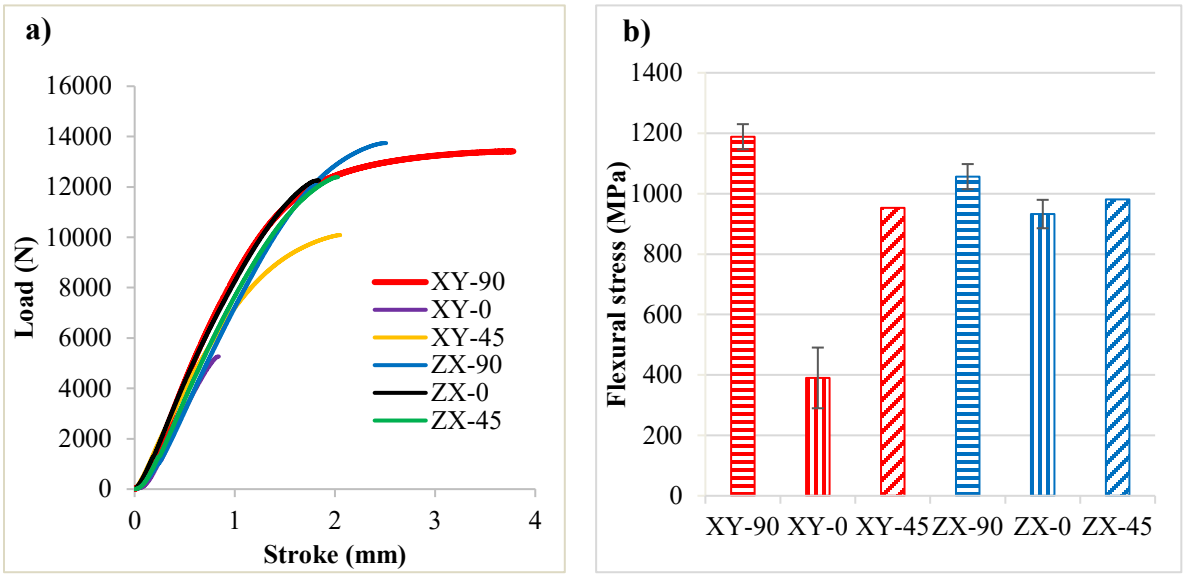

Fig. 4 *a) Curves load-stroke b) Comparison of the average maximum flexural stress and their standard deviation*

In Fig. 4a were reported the comparison of the average maximum σ_f obtained from the tests. In Fig. 4b was selected and reported the curves load-stroke of the specimens that with the highest load for each group. Fig. 4b showed how XY-90 was the better configuration, with a maximum flexural stress of 1188.3±41.7 MPa, followed by ZX-90 with a σ_f of 1056.3±41.6 MPa. The weakest group, as was the XY-0 (390.1±100.4 MPa). This was due to the orientation of the raster that negatively affected the specimens causing a delamination. All the other groups, independently from printing direction, reported a σ_f above the 950 MPa. The flat specimens did not break at the end of the test but reported a crack at the bottom surface where the tensile force acted (Fig. 5a-b). Differently for the upright, where the end of the test occurred when the specimens broke with a delamination of the layers (Fig. 5c-d). More evident the differences between XY-0 (a) and XY-90 (b), with the first one undeformed-like compared to the second one. The presence of lacks adhesion between infill and wall lines for ZX-0 specimen (c) were well showed. This defect could be the main cause to a lower flexural stress compared to the ZX-90 (d), where the cross-section appeared denser, also confirmed by the values of density in Table 3 (7.4 g/cm^3 > 7.1 g/cm^3).

Materials Research Proceedings 35 (2023) 135-142 https://doi.org/10.21741/9781644902714-17

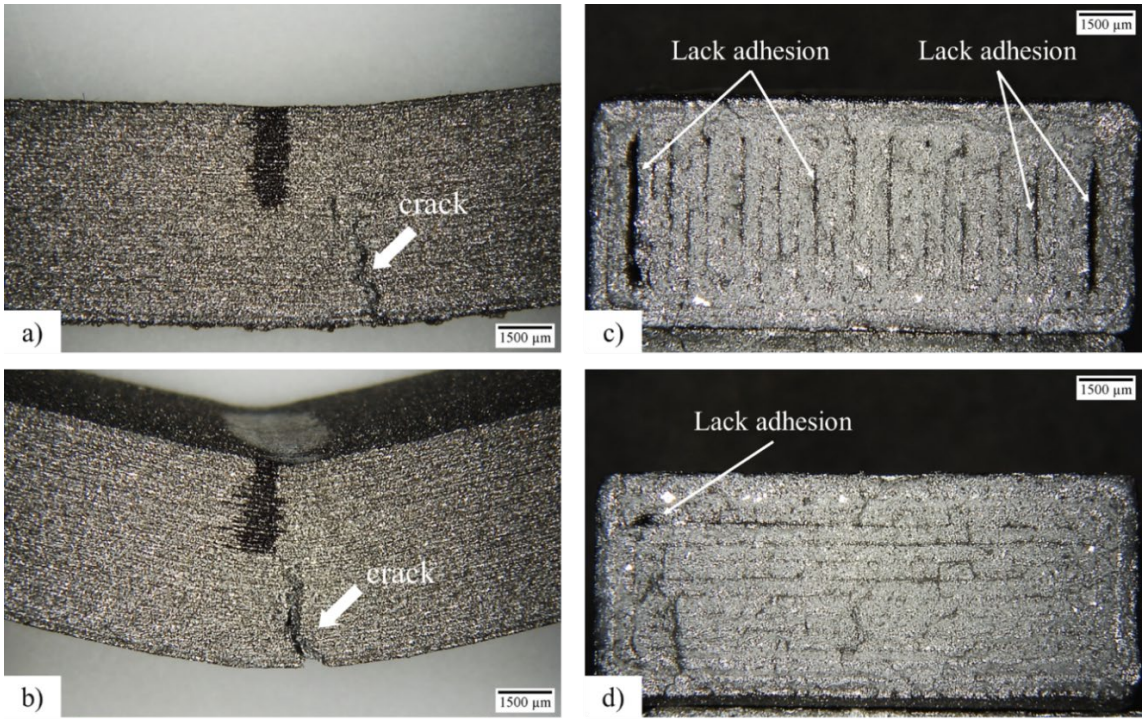

Fig. 5 *Bended specimens: a) XY-0 b) XY-90 and fracture surfaces of c) ZX-0 d) ZX-90*

More in detail the effect of the printing direction and infill line strategy on the bending properties a statistical analysis was investigated. The one-way ANOVA approach was considered using a confident interval of 95% (α=0.05).

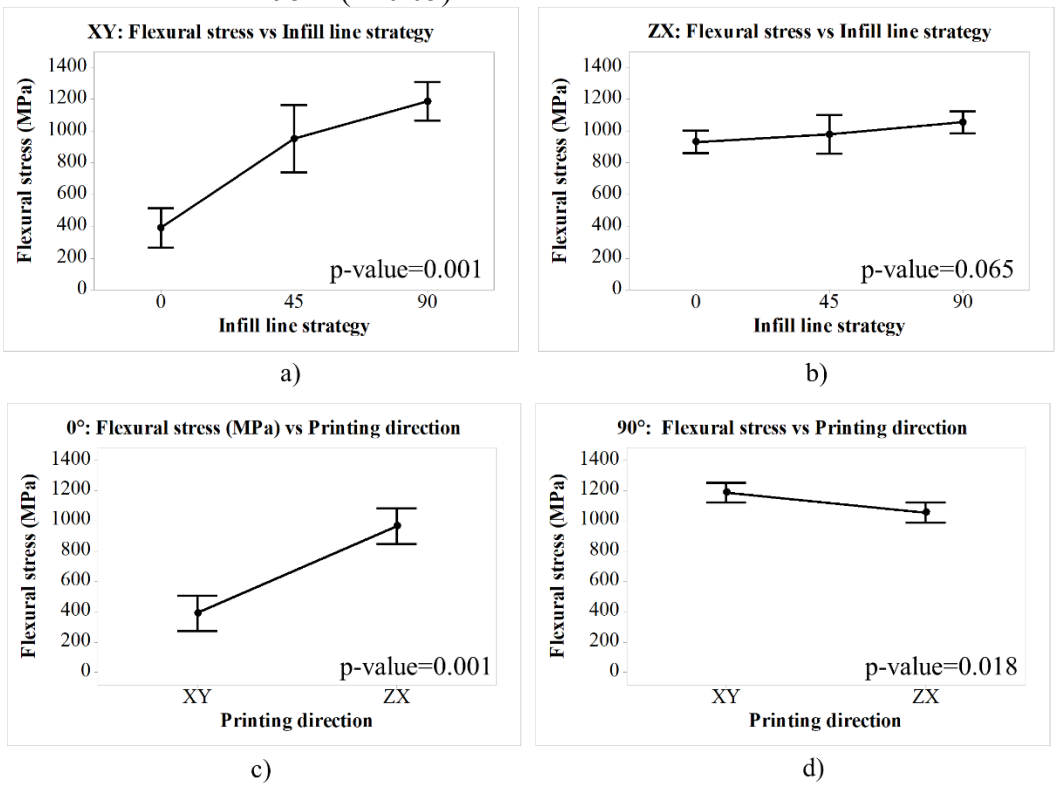

Fig. 6 *Boxplot for a) XY specimens b) ZX specimens of the maximum flexural stress for the different infill line strategy and c) 0° direction and d) 90° direction of the maximum flexural stress for the printing direction*

In Fig. 6a and Fig. 6b were showed the trend of flexural stress for the infill line strategies. The specimens +/-45° were insert for comparison, even if they were a single repetition. In Fig. 6a the trend reported for flat specimens highlighted how varying the infill line strategy from unidirectional 0° to +/-45° up to unidirectional 90° has led to increase the bending stress of about 3 times. This was supported by the results of one-way ANOVA, where the p-value was lower than 0.05. On the other hand, the specimens printed in upright (Fig. 6b), were not influenced by the infill line strategy, and confirmed by a p-value bigger than 0.05. In Fig. 6c and Fig. 6d were showed the boxplot of flexural stress for the two printing direction. Fig. 6c, showed how considering 0° line direction, the upright specimens obtained the highest values (σ_f of ZX≃2.5 times the σ_f of XY). The p-value ($0.001 << \alpha$) suggested how the printing orientation significantly affected the flexural stress for this type of infill line strategy. The specimens printed with an infill line strategy of 90°, appeared more similar as confirmed by the boxplot of Fig. 6d. However, the one-way ANOVA confirmed also in this case an influence of the printing orientation on the flexural stress.

Conclusions

In the present work, a commercial 17-4 PH filament was used to produce four kinds of bending specimens in order to evaluate the influence of the variation of printing direction and infill line strategy on the density of the printed and sintered part and on flexural stress of the sintered parts. The results obtained were reported below:

- The densities in the green and sintered condition of the parts with a unidirectional infill line strategy were lower than +/-45° specimens. The Pareto chart confirmed the influence of the printing direction on the green and sintered density. The sintered density was influenced by defects induced by the sintering process.
- The bending test revealed a significant influence of the parameters on the flexural stress. The best group was the XY-90 with 1188.3±41.7 MPa of flexural stress, instead the worst one was the XY-0 with 390.1±100.4 MPa. For the upright specimens not relevant differences, as confirmed by the one-way ANOVA for the infill line, emerged with a σ_f of 1056.3±41.6 MPa for ZX-90 and 932.5±47.0 MPa for ZX-0. The printing direction also influenced the bending stress, mainly when the infill line strategy 0° was considered.

References

[1] P. Parenti, D. Puccio, B.M. Colosimo, Q. Semeraro, A new solution for assessing the printability of 17-4 PH gyroids produced via extrusion-based metal AM, J. Manuf. Process. 74 (2022) 557–572. http://doi.org/10.1016/j.jmapro.2021.12.043

[2] M. Carminati, M. Quarto, G. D'urso, C. Giardini, G. Maccarini, Mechanical Characterization of AISI 316L Samples Printed Using Material Extrusion, Appl. Sci. 12 (2022). http://doi.org/10.3390/app12031433

[3] W. Lengauer, I. Duretek, M. Fürst, V. Schwarz, J. Gonzalez-gutierrez, S. Schuschnigg, C. Kukla, M. Kitzmantel, E. Neubauer, C. Lieberwirth, V. Morrison, Fabrication and properties of extrusion-based 3D-printed hardmetal and cermet components, Int. J. Refract. Metals Hard Mater. 82 (2019) 141–149. http://doi.org/10.1016/j.ijrmhm.2019.04.011

[4] M. Sadaf, M. Bragaglia, F. Nanni, A simple route for additive manufacturing of 316L stainless steel via Fused Filament Fabrication, J. Manuf. Process. 67 (2021) 141–150. http://doi.org/10.1016/j.jmapro.2021.04.055

[5] L.M. Galantucci, A. Pellegrini, M.G. Guerra, F. Lavecchia, 3D printing of parts using Metal Extrusion: an overview of Shaping Debinding and Sintering technology, Adv. Technol. Mater. 47 (2022) 25–32. http://doi.org/10.24867/ATM-2022-1-005

[6] J. Gonzalez-Gutierrez, S. Cano, S. Schuschnigg, C. Kukla, J. Sapkota, C. Holzer, Additive manufacturing of metallic and ceramic components by the material extrusion of highly-filled polymers: A review and future perspectives, Materials (Basel). 11 (2018). http://doi.org/10.3390/ma11050840

[7] F. Lavecchia, A. Pellegrini, L.M. Galantucci, Comparative study on the properties of 17-4 PH stainless steel parts made by metal fused filament fabrication process and atomic diffusion additive manufacturing, Rapid Prototyp. J. 29 (2023) 393–407. http://doi.org/10.1108/RPJ-12-2021-0350

[8] J. Gonzalez-gutierrez, S. Cano, J.V. Ecker, M. Kitzmantel, F. Arbeiter, C. Kukla, C. Holzer, Bending Properties of Lightweight Copper Specimens with Different Infill Patterns Produced by Material Extrusion Additive Manufacturing , Solvent Debinding and Sintering, Appl. Sci. (2021). http://doi.org/10.3390/app11167262

[9] P. Singh, V.K. Balla, S. V. Atre, R.M. German, K.H. Kate, Factors affecting properties of Ti-6Al-4V alloy additive manufactured by metal fused filament fabrication, Powder Technol. 386 (2021) 9–19. http://doi.org/10.1016/j.powtec.2021.03.026

[10] M.Á. Caminero, A. Romero, J.M. Chacón, P.J. Núñez, E. García-Plaza, G.P. Rodríguez, Additive manufacturing of 316L stainless-steel structures using fused filament fabrication technology: mechanical and geometric properties, Rapid Prototyp. J. 27 (2021) 583–591. http://doi.org/10.1108/RPJ-06-2020-0120

[11] G. Singh, J.M. Missiaen, D. Bouvard, J.M. Chaix, Copper additive manufacturing using MIM feedstock: adjustment of printing, debinding, and sintering parameters for processing dense and defectless parts, Int. J. Adv. Manuf. Technol. 115 (2021) 449–462. http://doi.org/10.1007/s00170-021-07188-y

[12] Y. Thompson, J. Gonzalez-Gutierrez, C. Kukla, P. Felfer, Fused filament fabrication, debinding and sintering as a low cost additive manufacturing method of 316L stainless steel, Addit. Manuf. 30 (2019) 100861. doi:10.1016/j.addma.2019.100861.

[13] C. Suwanpreecha, A. Manonukul, On the build orientation effect in as-printed and as-sintered bending properties of 17-4PH alloy fabricated by metal fused filament fabrication, Rapid Prototyp. J. 28 (2022) 1076–1085. http://doi.org/10.1108/RPJ-07-2021-0174

[14] T.C. Henry, M.A. Morales, D.P. Cole, C.M. Shumeyko, J.C. Riddick, Mechanical behavior of 17-4 PH stainless steel processed by atomic diffusion additive manufacturing, Int. J. Adv. Manuf. Technol. 114 (2021) 2103–2114. http://doi.org/10.1007/s00170-021-06785-1